at the attachment organelle. These HMW proteins are present in high concentrations at the attachment organelle and are thought to be the most likely components of the electron-dense core (3, 25, 48, 49, 52). HMW1 and HMW3 are encoded in the *hmw* operon, and the gene encoding HMW2 is in the *crl* operon (24). In addition to these cytadherence-related proteins, the Triton X-100-insoluble fraction contains proteins P65 and P200. P65 and P200 share a structural domain, the acidic proline-rich domain, with HMW1 and HMW3 (40, 41). The structural similarity suggests that proteins P65 and P200 have roles similar to those of HMW1 and HMW3 as components of cytoskeleton-like structures. However, it is not clear whether proteins P65 and P200 participate in cytadherence. Recent studies revealed that P65 localizes to the attachment organelle with P30, an additional adhesin protein that is an essential factor for cytadherence (2, 20, 25, 48, 49). The genes encoding P65 and P30 are located in the *crl* and *hmw* operons, respectively. The gene encoding P200 is not located in one of the three operons of cytadherence-related proteins (2, 24).

Although these candidate components of the attachment organelle and cytoskeleton-like structures have been identified, the spatial configuration and interaction between these proteins are poorly understood. Antibodies have been used to localize specific proteins to the attachment organelle (46, 48, 49, 52), but their use is limited because of the need for specificity of an antibody for a target protein and the inability to observe living systems in real time. Green fluorescent protein (GFP), an intrinsically fluorescent molecule obtained from the jellyfish *Aequorea victoria*, is widely used to study protein-protein interactions, cell division, and gene expression in a variety of organisms in real time (39, 50). In this study, we developed a dual GFP expression system for *M. pneumoniae* to study the spatial relationship of P65 to HMW2, P41, and P24, which are encoded in the *crl* operon (28).

MATERIALS AND METHODS

Organism and culture conditions. The *M. pneumoniae* strains listed in Table 1 were cultured in PPLO medium (2.1% PPLO broth [Becton Dickinson, Sparks, Md.], 0.25% glucose, 0.002% phenol red, 0.5% yeast extract [Becton Dickinson], 10% horse serum [Gibco BRL, Rockville, Md.], 50 μg of ampicillin/ml) or in Aluotto medium (1, 38) at 37°C. For drug-resistant *M. pneumoniae* strains, 18 μg of gentamicin/ml or 15 μg of chloramphenicol/ml was added to the media. *Escherichia coli* JM83 (53), DH5α (13), and DB3.1 (Invitrogen, Carlsbad, Calif.) were used as host strains to construct plasmids and were grown in Luria-Bertani medium (47) with or without 50 μg of ampicillin/ml, 50 μg of kanamycin/ml, and 15 μg of chloramphenicol/ml at 37°C.

Construction of fusion genes and plasmids. The synthetic oligonucleotides used for plasmid construction are listed in Table 2. *M. pneumoniae* M129 genomic DNA was prepared by a conventional phenol extraction method. The *p65* gene was amplified from the genomic DNA by PCR with primers P65F-Bam and P65R-Nco. To minimize mutations caused by PCR amplification, high-fidelity DNA polymerase PyroBest (Takara, Tokyo, Japan) was used. The amplified fragment was digested with BamHI and NcoI and was inserted into the BamHI-NcoI site (the 5′ end of the *eyfp* gene) of plasmid pEYFP (Clontech, Palo Alto, Calif.), producing a plasmid that we designated pTK150. The *p65* gene was also amplified from the genomic DNA by PCR with primers P65F-Bsr and P65R-Eco. The amplified fragment was inserted into the BsrGI-EcoRI site (the 3′ end of the *eyfp* gene) of plasmid pEYFP after digestion with BsrGI and EcoRI, producing a plasmid that we designated pTK153. The *p65-eyfp* and *eyfp-p65* fusion genes were excised from plasmids pTK150 and pTK153 by using PvuII and StuI and were inserted into the SmaI site of plasmid pISM2062.2 (22), producing plasmids pTK155 and pTK158, respectively (Table 3). Plasmids pTK161 and pTK162 (Table 3) were constructed by replacing the *E. coli lac* promoter sequence in pTK158 (derived from plasmid pEYFP) with *p65* or *tuf* promoter fragments from *M. pneumoniae* at the BamHI-NcoI site. The *p65* and *tuf* promoter fragments were obtained from *M. pneumoniae* genomic DNA by PCR with primers P65F-Bam and P65-PR and primers tuf-PF and tuf-PR, respectively. These promoter fragments were also used to replace the *p65* gene and its promoter sequence in pTK155 at the BamHI-NcoI site. The resulting plasmids, which expressed the *eyfp* gene alone from the *p65* and *tuf* promoters, were designated pTK164 and pTK165, respectively (Table 3).

TABLE 1. *M. pneumoniae* strains used in this study[a]

Strain	Description[b]
M129	Wild type
TK2062	M129(pISM2062.2)
TK155	M129(pTK155)
TK161	M129(pTK161)
TK162	M129(pTK162)
TK164	M129(pTK164)
TK165	M129(pTK165)
TK210	M129(pTK210)
TK2100	TK210(pISM2062.2)
TK2310	TK210(pMPN310)
TK2311	TK210(pMPN311)
TK2312	TK210(pMPN312)
TK2310T	TK210(pMPN310-tuf)
TK2311T	TK210(pMPN311-tuf)
TK2312T	TK210(pMPN312-tuf)
TK3310	M129(pMPN310)
TK3311	M129(pMPN311)
TK3312	M129(pMPN312)
TK3310T	M129(pMPN310-tuf)
TK3311T	M129(pMPN311-tuf)
TK3312T	M129(pMPN312-tuf)

[a] All strains were designed in this study, except for the wild-type strain (31).
[b] Tn*4001* plasmids were used to transform *M. pneumoniae*.

The *ecfp* gene was amplified from plasmid pECFP (Clontech) by PCR with primers CFP1F-Sma and CFP-R. The amplified *ecfp* fragment was inserted into the SmaI site of pKV104, producing a plasmid that we designated pTK205. pKV104 contains a chloramphenicol-resistant (Cm^r) variant of Tn*4001* (12) and was kindly provided by D. C. Krause of the University of Georgia. The *lac* promoter region of pTK205 (upstream of the *ecfp* gene) was replaced at the SmaI-AgeI site with the *M. pneumoniae tuf* promoter sequence amplified by PCR with primers tuf-F and tufR-Age, resulting in plasmid pTK207. The BsrGI site of pTK207 (the 3′ end of the *ecfp* gene) was converted to an EcoRV site with an oligonucleotide linker, 160RVS. Next, the Gateway vector conversion system (reading frame cassette A) (Invitrogen) was inserted into the EcoRV site, producing a plasmid that we designated pTK207-D. The *p65* gene was amplified from *M. pneumoniae* genomic DNA with primers MPN309-F-Gw and MPN309-R-Gw, subcloned into plasmid pDONR201 (Invitrogen) by using BP clonase (Invitrogen), and then transferred to plasmid pTK207-D by using LR clonase (Invitrogen); this procedure produced plasmid pTK210 (Table 3).

Plasmids containing *hmw2*, *p41*, and *p24* fusion genes were constructed as follows. The BsrGI site of plasmid pTK164 and that of plasmid pTK165 were converted to an EcoRV site by inserting an oligonucleotide linker, 160RVS. Next, the Gateway vector conversion system (reading frame cassette A) was inserted in the created EcoRV site, producing plasmids pTK164-D and pTK165-D. The *hmw2* gene sequence was amplified from *M. pneumoniae* genomic DNA by PCR with primers MPN310-F-Not and MPN310-R-Asc. After digestion with NotI and AscI, the *hmw2* gene fragment was inserted into the NotI-AscI site of plasmid pENTR/D-TOPO (Invitrogen), resulting in a plasmid that we designated pMPN310-E. The *p41* and *p24* gene sequences were amplified from *M. pneumoniae* genomic DNA by PCR with primers MPN311-F-Gw and MPN311-R-Gw and primers MPN312-F-Gw and MPN312-R-Gw, respectively. The amplified fragments were subcloned into plasmid pDONR201 by using BP clonase, producing plasmids that we designated pMPN311-E and pMPN312-E. The *hmw2*, *p41*, and *p24* gene fragments of plasmids pMPN310-E, pMPN311-E, and pMPN312-E were transferred to plasmids pTK164-D and pTK165-D by using LR clonase. The resulting plasmids (pMPN and pMPN-tuf series), which are listed in Table 3, were used to transform *M. pneumoniae*.

Transformation of *M. pneumoniae*. *M. pneumoniae* with the modified Tn*4001* (Tn*4001*mod) plasmids was transformed by the electroporation method described by Hedreyda et al. (15). The transformed cells were grown in liquid PPLO medium containing 18 μg of gentamicin/ml or 15 μg of chloramphenicol/

TABLE 2. Synthetic oligonucleotides used in this study

Oligonucleotide	Sequence[a]
P65F-Bam	GCGGGATCCTGCAGCAGCTGACAACAACATTTAGCACACT
P65R-Nco	CTAGCCATGGCTTCGTAAAATTCATCACCAC
P65F-Bsr	GAGCTGTACAAGATGGATATAAATAAACCAGG
P65R-Eco	TCGCGGAATTCAGCTGTTTATTCGTAAAATTCATCACCAC
P65-PR	CAACCCATGGCATTTATATCCATTTACTGTCT
tuf-PF	GTGGGATCCATTTTGCAAACTGATGACAA
tuf-PR	TAACCATGGGTTTAGATCGGTCAAATTT
CFP1F-Sma	GATCCCGGGAGCGCCCAATACGCAAACCGCC
CFP-R	CCTATTATTTTTGACACCAGAC
165RVS	GTACGATATC
tuf-F	ATTTTGCAAACTGATGACAA
tufR-Age	TCGGACCGGTTTCTCTCTTGCCATGTGTTTG
MPN309-F-Gw	GGGGACAAGTTTGTACAAAAAAGCAGGCTTCATGGATATAAATAAACCAGGTTGAA
MPN309-R-Gw	GGGGACCACTTTGTACAAGAAAGCTGGGTTATTATTCGTAAAATTCATCACCAC
MPN310-F-Not	CCGCGGCCGCCATGAATGATACTGACAAGAAGT
MPN310-R-Asc	GTCGGCGCGCCCTTATTTAGCTGCTTTTTGGGC
MPN311-F-Gw	GGGGACAAGTTTGTACAAAAAAGCAGGCTTCATGACTAATGATTACCAACAATTAAA
MPN311-R-Gw	GGGGACCACTTTGTACAAGAAAGCTGGGTATCCTTCATTACTTTGTTCT
MPN312-F-Gw	GGGGACAAGTTTGTACAAAAAAGCAGGCTTCATGAAGGATAGTGCACTAACACT
MPN312-R-Gw	GGGGACCACTTTGTACAAGAAAGCTGGGTTACTTCTTGTAAGAAATTAAC

[a] Recognition sites for restriction enzymes and the *att* sites for recombinase are underlined.

ml. The transformation efficiencies were checked by counting the transformant colonies on PPLO agar plates. To minimize the positional effect of Tn*4001*mod insertion in the comparisons of the transformants, we analyzed and compared the transformant strains as a whole transformed population without picking up a single colony.

Protein analysis. *M. pneumoniae* cells were grown in tissue culture flasks to the mid-log phase and were scraped from the bottom of the flasks. The cells were collected by centrifugation at 20,000 × *g* for 15 min at 4°C and washed three times with phosphate-buffered saline. The final cell suspension, adjusted to a total protein concentration of 1 μg/μl, was lysed by adding sample loading buffer and was subjected to sodium dodecyl sulfate (SDS)-polyacrylamide gel electrophoresis (PAGE) at a load of 5 or 10 μg of total protein per lane (47). For Western blot analysis, the separated proteins were transferred to a nitrocellulose membrane (Bio-Rad, Hercules, Calif.). Monoclonal antibody JL-8 (specific for *A. victoria* GFP variants) (Clontech) was used at a 1:2,000 dilution to detect enhanced yellow fluorescent protein (EYFP) and enhanced cyan fluorescent protein (ECFP). Anti-P65 antiserum (49) was also used at a 1:2,000 dilution. The reacting antibodies were detected with an alkaline phosphatase-conjugated second antibody (goat anti-mouse immunoglobulin G) (Promega, Madison, Wis.) and 5-bromo-4-chloro-3-indolylphosphate (BCIP)–nitroblue tetrazolium (NBT) color development substrate (Promega) according to manufacturer instructions.

Microscopy. *M. pneumoniae* strains were cultured in Aluotto medium at 37°C to the mid-log phase. Cytadherence-positive cells were scraped from the bottom of the culture flasks after the medium was replaced with a volume of fresh medium that was two to five times smaller. The cell suspension was passed through a 25-gauge needle several times, filtered through a membrane filter unit

TABLE 3. Plasmids constructed in this study[a]

Plasmid	Vector	Marker	Promoter	Gene	Expression[b]	Fluorescence[c]	Localization[d]
pTK150	pEYFP	Ap^r	*p65*	*p65-eyfp*	NT	NT	NT
pTK153	pEYFP	Ap^r	*lac* (*E. coli*)	*eyfp-p65*	NT	NT	NT
pTK155	pISM2062.2	Ap^r Gm^r	*p65*	*p65-eyfp*	+	+	+
pTK158	pISM2062.2	Ap^r Gm^r	*lac* (*E. coli*)	*eyfp-p65*	−	−	−
pTK161	pISM2062.2	Ap^r Gm^r	*p65*	*eyfp-p65*	+	+	+
pTK162	pISM2062.2	Ap^r Gm^r	*tuf*	*eyfp-p65*	++	++	+
pTK164	pISM2062.2	Ap^r Gm^r	*p65*	*eyfp*	+	+	−
pTK164-D	pISM2062.2	Ap^r Gm^r Cm^r	*p65*	*eyfp*	NT	NT	NT
pTK165	pISM2062.2	Ap^r Gm^r	*tuf*	*eyfp*	++	++	−
pTK165-D	pISM2062.2	Ap^r Gm^r Cm^r	*tuf*	*eyfp*	NT	NT	NT
pTK205	pKV104	Ap^r Cm^r	*lac* (*E. coli*)	*ecfp*	NT	NT	NT
pTK207	pKV104	Ap^r Cm^r	*tuf*	*ecfp*	++	++	−
pTK207-D	pKV104	Ap^r Cm^r	*tuf*	*ecfp*	NT	NT	NT
pTK210	pTK207-D	Ap^r Cm^r	*tuf*	*ecfp-p65*	++	++	+
pMPN310-E	pENTR/D-TOPO	Km^r	None	*hmw2*	NT	NT	NT
pMPN311-E	pDONR201	Km^r	None	*p41*	NT	NT	NT
pMPN312-E	pDONR201	Km^r	None	*p24*	NT	NT	NT
pMPN310	pTK164-D	Ap^r Gm^r	*p65*	*eyfp-hmw2*	+	+	+
pMPN311	pTK164-D	Ap^r Gm^r	*p65*	*eyfp-p41*	+	+	+
pMPN312	pTK164-D	Ap^r Gm^r	*p65*	*eyfp-p24*	+	+	+
pMPN310-tuf	pTK165-D	Ap^r Gm^r	*tuf*	*eyfp-hmw2*	++	++	+
pMPN311-tuf	pTK165-D	Ap^r Gm^r	*tuf*	*eyfp-p41*	++	++	+
pMPN312-tuf	pTK165-D	Ap^r Gm^r	*tuf*	*eyfp-p24*	++	++	+

[a] *M. pneumoniae* strains transformed with Tn*4001* plasmids were analyzed by Western blotting and fluorescence microscopy. NT, not applicable or not tested.
[b] Expression of the fusion protein in *M. pneumoniae* cells was monitored by Western blotting: +, ++, and −, moderate, strong, and no expression, respectively.
[c] Fluorescence intensity was observed by microscopy: +, ++, and −, faint, strong, and no fluorescence, respectively.
[d] Localization of the fusion protein at cell poles was observed by microscopy; +, present; −, absent.

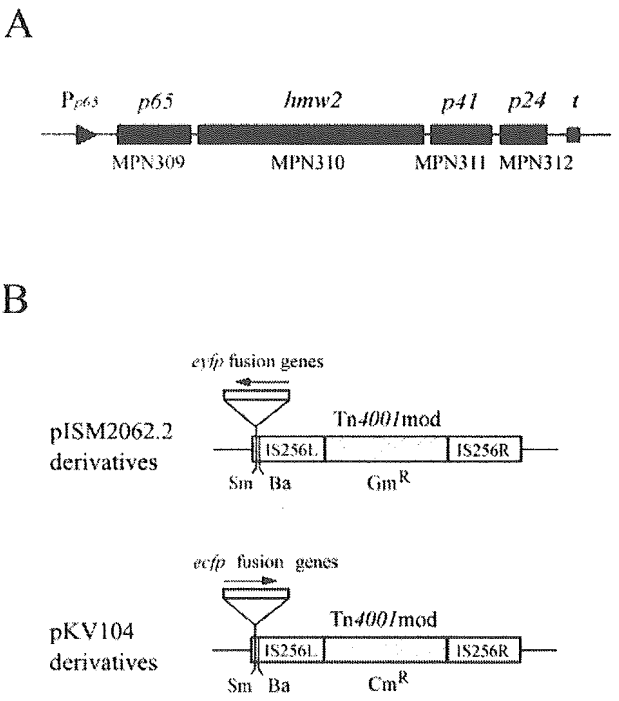

FIG. 1. (A) Schematic illustration of the *crl* operon of *M. pneumoniae*. The four rectangular bars indicate the *p65*, *hmw2*, *p41*, and *p24* genes in this operon. These genes are also designated MPN309, MPN310, MPN311, and MPN312 according to the serial numbering system of the *M. pneumoniae* genome project (8). The triangle and the square represent the *p65* promoter (P_{p65}) and the terminator (*t*) of this operon, respectively. The figure is not drawn precisely to scale. (B) Structures of modified staphylococcal transposon Tn*4001*mod vectors (11, 22). Plasmid pISM2062.2 carries a Gm^r version of Tn*4001*mod. Plasmid pKV104 carries a Cm^r version of Tn*4001*mod. The IS256L, IS256R, and drug resistance genes (Gm^r and Cm^r) of Tn*4001*mod are illustrated. Cloning sites (Sm, SmaI; Ba, BamHI) in Tn*4001*mod are indicated. The *eyfp* fusion genes were inserted into the SmaI site of pISM2062.2. The *ecfp* fusion genes were inserted into the SmaI site of pKV104. The arrows indicate the directions in which the fusion genes were inserted.

with a 0.45-μm-pore size (Millipore, Billerica, Mass.) to disperse aggregates (46, 48), and placed on coverslips cleaned with saturated ethanolic KOH (4). The coverslips with the cell suspensions were incubated at 37°C for 0.5 to 1 h and were mounted on glass slides after excess cell suspensions were removed. To observe ECFP fluorescence, coverslips were washed twice with phosphate-buffered saline before being mounted on glass slides to reduce background fluorescence. The cells were observed with a BX51 fluorescence microscope equipped with YFP and CFP filter units (U-MYFPHQ and U-MCFPHQ, respectively) and a phase-contrast setup (Olympus, Tokyo, Japan). The images were digitized by using a Photometrics CoolSNAPcf charge-coupled device camera (Roper Scientific, Atlanta, Ga.) and LuminaVision software (Mitani Corp., Tokyo, Japan); signals were adjusted to obtain proper intensities. The fluorescence images were pseudocolored by using the LuminaVision software. The images were also processed by using Adobe Photoshop software, versions 6.0 and 7.0 (Adobe Systems, San Jose, Calif.).

To observe gliding, cells of strain TK162 were suspended in saline containing 20% horse serum. The cell suspension was inserted into a tunnel that was 12 mm wide, 18 mm long, and 0.06 mm high and that was assembled from a glass slide, a coverslip, and two pieces of double-sided tape; the cells were incubated in this tunnel for 10 min at 37°C. The cells then were observed with the fluorescence microscope at 37°C; this temperature was achieved by attaching a heating system to the sample stage and the objective lens. Cell images were recorded by using a charge-coupled device camera (WV-BP510; Panasonic, Osaka, Japan) and a digital videocassette recorder (WV-D9000; Sony, Tokyo, Japan) and were digitized as described previously (37).

RESULTS

Construction of the *p65* fusion genes and their expression in *M. pneumoniae* cells. We chose the P65 protein as the initial target for the fluorescent-protein tagging strategy by virtue of the location of its gene just downstream of the promoter of the *crl* operon (28) (Fig. 1A); this promoter can be used to express recombinant *p65* genes. The *eyfp* gene, encoding EYFP, which is a yellow-green-shifted variant of GFP that gives a stronger fluorescence emission than the wild type (10), was fused to the 3′ or 5′ end of the *p65* gene. The fusion genes were under the control of the native *p65* promoter and were inserted into the SmaI site of Tn*4001*mod vector plasmid pISM2062.2 (22) (Fig. 1B). The plasmids that we designated pTK155 and pTK161 carry the *p65-eyfp* and *eyfp-p65* fusion genes, respectively (Table 3). These plasmids were introduced into *M. pneumoniae* M129 by electroporation to deliver fusion genes to the chromosome by the transposition of Tn*4001*mod. Transformants TK155 and TK161 (named for plasmids pTK155 and pTK161, respectively) were obtained and were examined by fluorescence microscopy, which detected faint fluorescent signals from both strains. In most cells, the signals were located at one pole (Fig. 2), suggesting that the P65-EYFP and EYFP-P65 fusions were produced in these strains and localized at the attachment organelle. The intensities of the fluorescence signals were similar between the strains but slightly stronger in TK161 (Fig. 2).

To enhance the fluorescence intensity, we chose the *eyfp-p65* fusion gene, which exhibited slightly brighter fluorescence, and

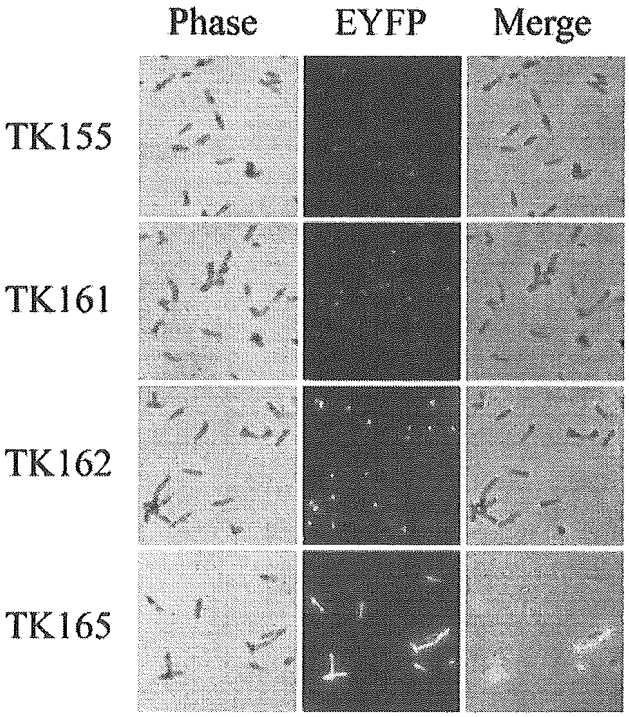

FIG. 2. Subcellular localization of EYFP fusions. The left and middle panels in each row show the same cells observed by phase-contrast microscopy and fluorescence microscopy, respectively. The right panel in each row shows the merged image of the left and middle panels. The transformants are named at left. Bar, 5 μm.

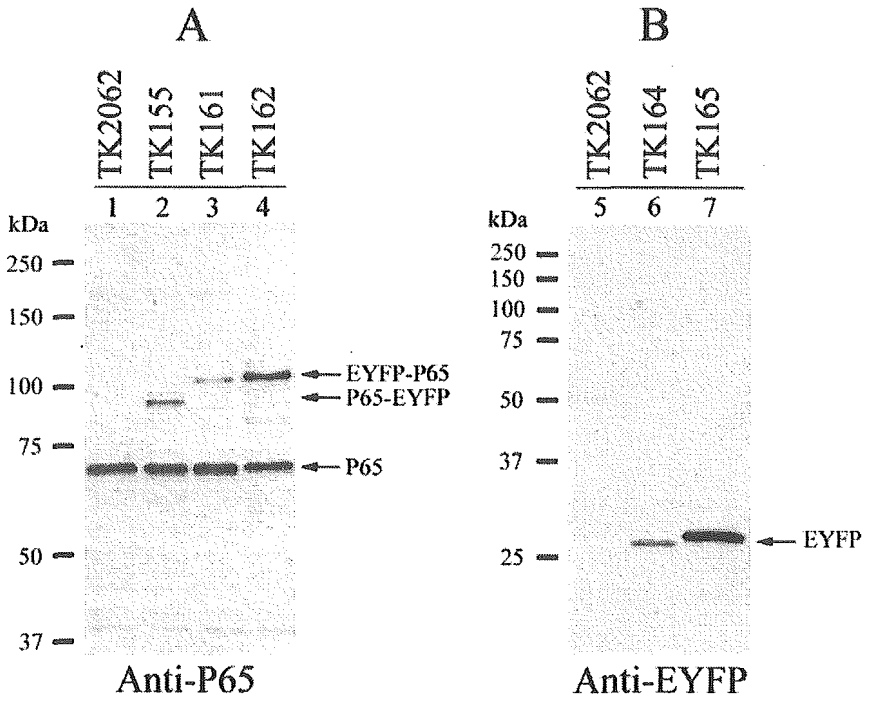

FIG. 3. Expression of fusions of P65 and EYFP in *M. pneumoniae* cells. (A) Western blot analysis of *M. pneumoniae* transformants with an anti-P65 antibody. Lysates of *M. pneumoniae* transformant cells (5 μg of total protein) were separated by SDS–8% PAGE, transferred to a nitrocellulose membrane, and probed with an anti-P65 antibody. The positions of the detected P65-EYFP, EYFP-P65, and native P65 are indicated by arrows. Molecular sizes are shown at left. The analyzed transformants are shown above the lanes. (B) Detection of EYFP expression by Western blot analysis. Lysates of *M. pneumoniae* transformant cells (5 μg of total protein) were separated by SDS–12% PAGE. The position of EYFP detected by an anti-EYFP (anti-GFP variant) antibody is indicated by an arrow. Molecular sizes are shown at left. The analyzed transformants are shown above the lanes.

we tested a promoter sequence of the *tuf* gene of *M. pneumoniae* instead of the *p65* promoter. Plasmid pTK162, which carries the *eyfp-p65* fusion gene under the control of the *tuf* promoter, was constructed and used to transform *M. pneumoniae* M129. The strain obtained, TK162, showed strong fluorescent signals at the cell poles (Fig. 2), suggesting higher production of the EYFP-P65 fusion in TK162 than in TK161. To confirm whether the polar localization of fusion proteins depends on the P65 moiety, we constructed plasmids pTK164 and pTK165, which carried the *eyfp* gene alone under the control of the *p65* or the *tuf* promoter (Table 3). The transformants with these plasmids, TK164 and TK165, showed fluorescence throughout the whole cell body (Fig. 2; only TK165 is shown), indicating that the polar localization of the P65-EYFP and EYFP-P65 fusions is caused by the properties of the P65 moiety. The intensity of EYFP fluorescence was strong in TK165 but faint in TK164, corresponding to their promoter activities.

We next analyzed transformant strains by Western blot analysis to examine the levels of expression of fusion proteins. By using anti-P65 antiserum, we detected P65-EYFP in TK155 and EYFP-P65 in both TK161 and TK162 (Fig. 3). TK155 and TK161 both had lower levels of fusion proteins than of native P65 (Fig. 3, lanes 2 and 3). On the other hand, the level of expression of EYFP-P65 in TK162 was comparable to that of native P65 (Fig. 3, lane 4). The size difference between P65-EYFP and EYFP-P65 (Fig. 3, lanes 2, 3, and 4) was caused by the addition of a short amino acid sequence at the N terminus of EYFP-P65, which resulted from the construction of the promoter fusion. The anti-EYFP antibody detected EYFP in both TK164 and TK165 (Fig. 3, lanes 6 and 7). The level of EYFP was low in TK164 but high in TK165, reflecting the activities of the *p65* and *tuf* promoters. The size difference for EYFP between TK164 and TK165 was attributed to the construction of the promoter fusion. These results indicated that the fluorescence intensities of the transformants correlated with their levels of EYFP fusion expression.

The fluorescence diminished in 10 s even in TK165 cells, with the highest intensity. This rather rapid bleaching may be attributable to the small number of fluorescent molecules caused by the small dimensions of *M. pneumoniae* cells. An *M. pneumoniae* cell is about 2 μm in length and 0.2 μm in diameter. The total volume is estimated to be 25 times lower than that of an *E. coli* cell. The signal from the small number of fluorescent molecules may easily fall below the detection limit as a result of photobleaching of the molecules.

The cytadherence ability of the transformants was also analyzed by a standard hemadsorption (HA) assay (14, 27). Of the colonies tested, 97% showed HA activity, suggesting that the expression of the EYFP fusions did not disturb the cytadherence processes of *M. pneumoniae*. However, 3% of the colonies did not show HA activity. This frequency of HA-negative colonies, obviously higher than that caused by spontaneous mutation (27), may have been caused by the insertion of Tn*4001* into the cytadherence-related genes.

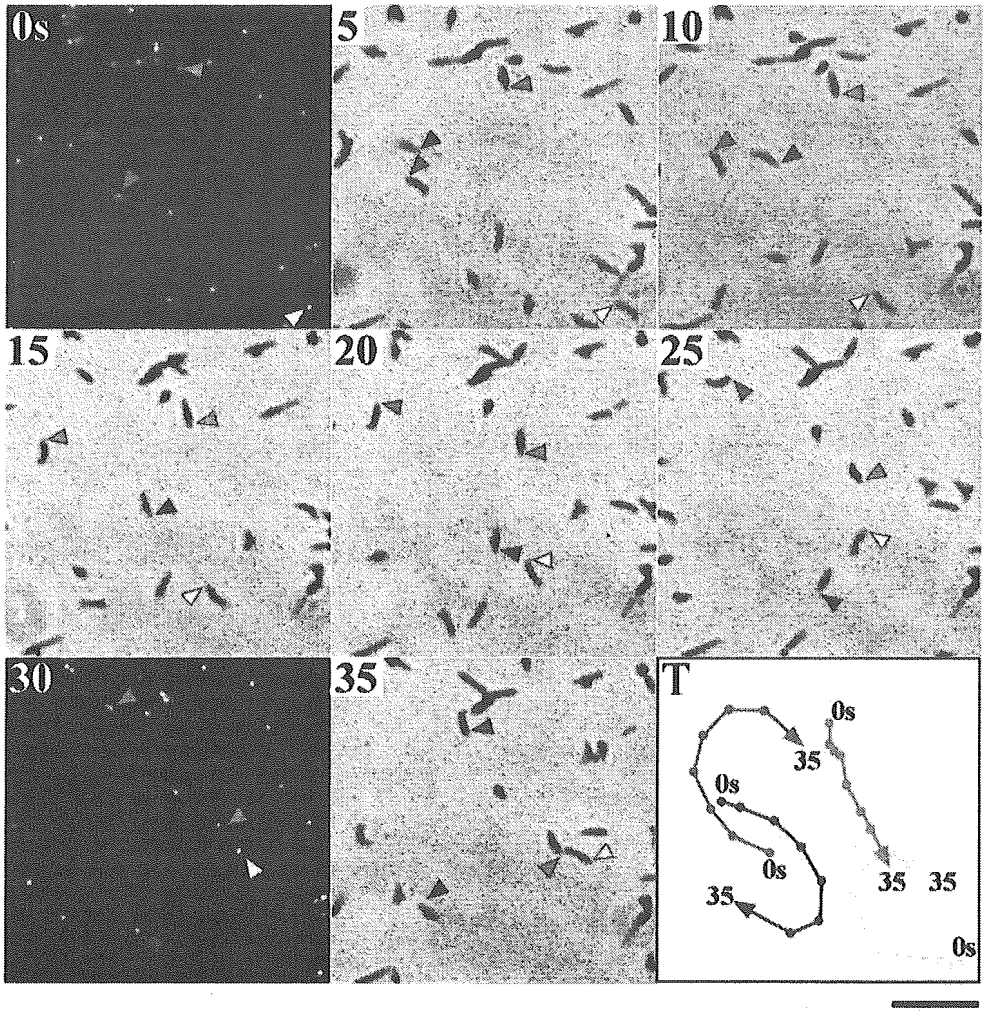

FIG. 4. Gliding motility of *M. pneumoniae* cells whose attachment organelles are fluorescently labeled with the EYFP-P65 fusion. Strain TK162 was observed by phase-contrast microscopy and fluorescence microscopy at 37°C. The phase-contrast image was recorded continuously with a video recorder. The microscope was shifted to the fluorescence setup for 2 s at 28-s intervals. The time intervals between images in this figure are 5 s. The positions of attachment organelles of four typical cells are indicated by colored arrowheads. The tracks of cell movement (positions of attachment organelles) are shown by colored lines in the bottom right panel (T). Bar, 5 μm.

Observation of gliding cells. Bredt (6, 7) and Radestock and Bredt (42) studied the gliding motility of *M. pneumoniae* cells by phase-contrast microscopy and concluded that the attachment organelle functions as the leading end of gliding cells. If EYFP-P65 fusions are properly incorporated into the attachment organelle, then the fluorescent foci must be observed at the leading end of gliding *M. pneumoniae* cells. To confirm this notion directly, we studied the gliding motility of TK162 cells, which exhibited the brightest fluorescent foci among the TK strains. To do so, we made slight modifications to a method used to observe the gliding of *Mycoplasma mobile* cells (35). TK162 cells were suspended in saline including 20% horse serum and were inserted into a tunnel assembled from a glass slide and a coverslip. We excluded heart infusion broth and yeast extract from the cell suspension, because these components of mycoplasma growth medium cause strong background fluorescence. The coverslip was maintained at 37°C on the microscope stage. Gliding cells on the glass surface and fluorescent foci were observed by phase-contrast microscopy and fluorescence microscopy, respectively (Fig. 4). As expected, the fluorescent focus was always positioned ahead of the gliding cell, indicating the localization of EYFP-P65 at the attachment organelle. In gliding cells, the attachment organelle (fluorescent focus) always moved smoothly, while the other part of the cell body often showed lateral wobble motion, consistent with previous observations (6, 7, 42). These results suggested that the organelle kept contact with the glass surface and that the other part of the cell body detached from the surface during gliding.

The proportion of gliding cells was apparently higher in saline containing 20% serum than in growth medium (unpublished data). Nutrient-starved conditions may accelerate the movement, as observed in other gliding bacteria (32). The addition of 1 to 5% gelatin was not needed with our conditions, although it has been reported to be essential for keeping cells on the glass surface (42). This difference may be related to differences in glass surface conditions between previous studies and our investigation.

The average speed of the gliding shown in Fig. 4 was calculated to be 0.40 μm/s, consistent with previous observations (6, 21, 42). We tried multiple times to observe the cell division process of *M. pneumoniae* during 30 min of continuous video recording but failed to find cells that exhibited nascent attachment organelle formation or cytokinesis.

Subcellular localization of the HMW2, P41, and P24 proteins. We extended the fluorescent-protein tagging strategy to the other gene products of the *crl* operon (the HMW2, P41, and P24 proteins) (Fig. 1A). Although the polar localization of HMW2 at the attachment organelle was reported recently by Balish et al. (3), the localization of P41 and P24 was unknown. For these experiments, we introduced a second fluorescent protein, ECFP (a blue-colored derivative of GFP) (10), to mark the positions of the attachment organelles of living cells. The *ecfp* gene was fused to the 5′ end of the *p65* gene and was under the control of the *tuf* promoter. This *ecfp-p65* fusion gene was introduced into *M. pneumoniae* M129 by use of a Cm^r derivative of Tn*4001*mod (11) (Fig. 1B). The resulting Cm^r transformant, which we designated TK210, expressed ECFP-P65 at a level slightly lower than that of native P65 (Fig. 5A) and exhibited blue fluorescent signals at the cell poles (attachment organelle) (Fig. 5B). We used TK210 as a host strain to examine the subcellular localization of HMW2, P41, and P24.

We constructed two groups of plasmids for the expression of EYFP fusions of HMW2, P41, and P24 by modifying plasmids pTK164 and pTK165 (Table 3). The first group of plasmids was designated pMPN (derivatives of pTK164); each of these plasmids possessed the *eyfp-hmw2*, *eyfp-p41*, or *eyfp-p24* fusion genes under the control of the *p65* promoter for low-level expression (Table 3). The second group of plasmids, designated pMPN-tuf (derivatives of pTK165) (Table 3), contained the *eyfp-hmw2*, *eyfp-p41*, or *eyfp-p24* fusion genes under the control of the *tuf* promoter for high-level expression. These plasmids were introduced into strain TK210, and Cm^r-Gm^r transformants were obtained. Western blot analysis for the fusion proteins confirmed that transformants TK2310, TK2311, and TK2312 (created with pMPN plasmids) expressed EYFP-HMW2, EYFP-P41, and EYFP-P24 at low levels (Fig. 6A), while transformants TK2310T, TK2311T, and TK2312T (created with pMPN-tuf plasmids) expressed them at higher levels (Fig. 6B). The EYFP fluorescent signals of strains with low-level expression were weak and were captured with an exposure time longer than that of strains with high-level expression (Fig. 7).

Strains TK2310 and TK2310T expressing EYFP-HMW2 showed fluorescent signals for EYFP at their cell poles. The distribution patterns for fluorescent foci were basically identical between the two strains, regardless of the level of expression of EYFP-HMW2, but the fluorescence signal intensities reflected the expression levels, as indicated by the difference in brightness between the focus signals and the background of the EYFP images (Fig. 7). In both strains, the fluorescent foci of EYFP-HMW2 almost overlapped those of ECFP-P65 (Fig. 7), indicating that the HMW2 protein was localized at the attachment organelle. These results confirmed the findings of Balish et al. (3).

Transformants TK2311, TK2312, TK2311T, and TK2312T revealed that EYFP-P41 and EYFP-P24 formed fluorescent foci in *M. pneumoniae* cells (Fig. 7). Unlike EYFP-HMW2, the

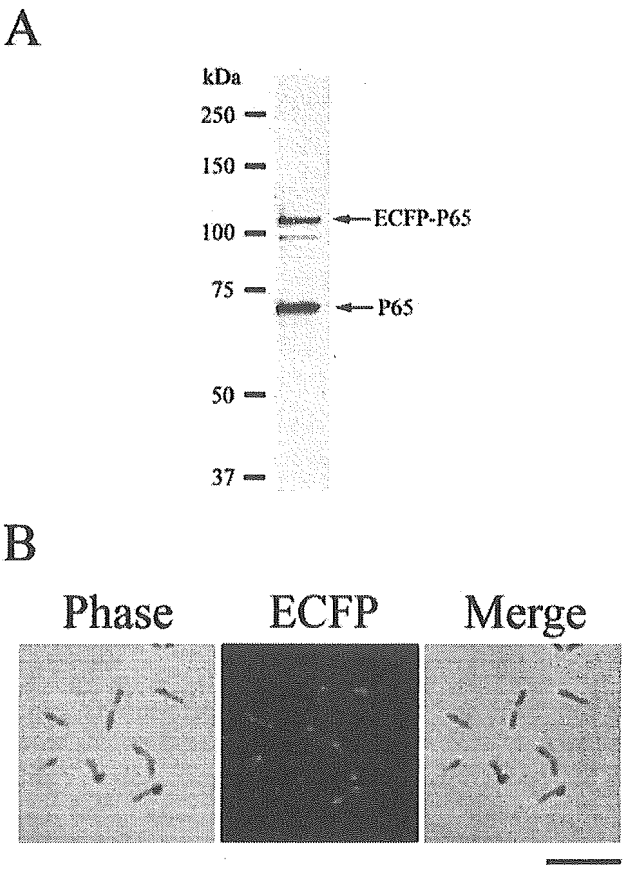

FIG. 5. Western blot analysis and fluorescence microscopy of *M. pneumoniae* TK210. (A) Western blot analysis of *M. pneumoniae* strain TK210. Lysates of *M. pneumoniae* TK210 cells (5 μg of total protein) were separated by SDS–8% PAGE, transferred to a nitrocellulose membrane, and probed with an anti-P65 antibody. The positions of the detected ECFP-P65 and native P65 are indicated by arrows. Molecular sizes are shown at left. (B) Subcellular localization of the ECFP-P65 fusion. The left and middle panels show the same cells observed by phase-contrast microscopy and fluorescence microscopy, respectively. The right panel shows the merged image of the left and middle panels. Bar, 5 μm.

foci of EYFP-P41 and EYFP-P24 were located mainly at the proximal region of the attachment organelle and did not overlap those of ECFP-P65. In strains showing low-level expression of EYFP-P41 or EYFP-P24 (TK2311 and TK2312), the fluorescent foci of these proteins were confined to the proximal end of the attachment organelle (Fig. 7), and the profiles of these proteins were very similar. However, in strains showing high-level expression (TK2311T and TK2312T), the distribution patterns for fluorescent signals were not identical between EYFP-P41 and EYFP-P24 (Fig. 7). In strain TK2311T, additional fluorescent foci for EYFP-P41 were frequently observed at the opposite end of the attachment organelle, i.e., at the cell tail (Fig. 7). On the other hand, the fluorescence signals for EYFP-P24 were diffused from the proximal end of the organelle to the cell tail (Fig. 7, TK2312T). These nonidentical distribution patterns for EYFP-P41 and EYFP-P24 in strains showing high-level expression suggested that these proteins had different properties in the cells. However, even in these strains showing high-level expression, the strongest signals

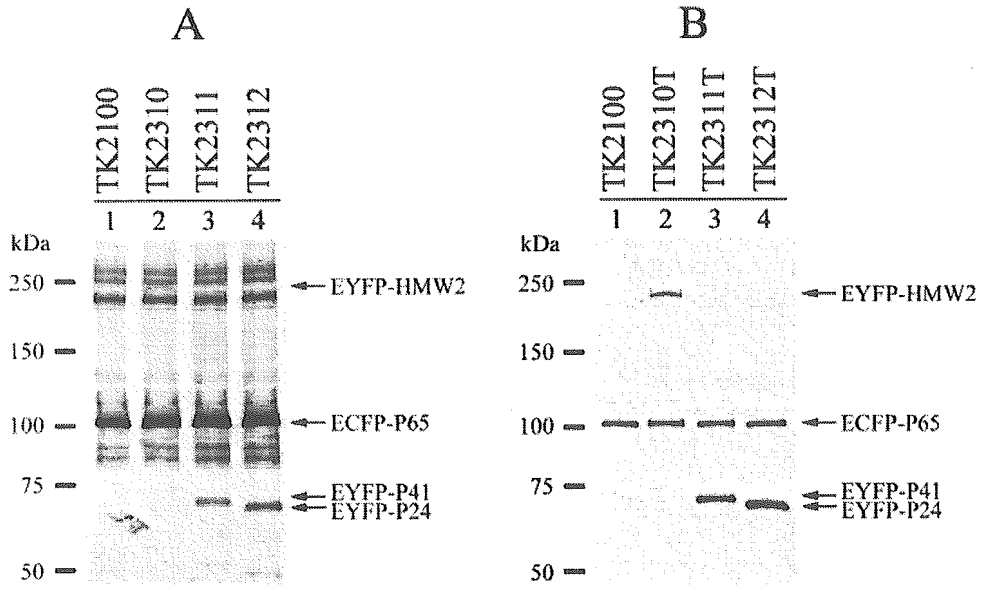

FIG. 6. Expression of EYFP-HMW2, EYFP-P41, and EYFP-P24 fusions in *M. pneumoniae* cells. (A) Western blot analysis of low-level expression transformants of EYFP fusions. Lysates of *M. pneumoniae* transformant cells (TK2100, TK2310, TK2311, and TK2312) (10 μg of total protein) were separated by SDS–5 to 10% gradient PAGE, transferred to a nitrocellulose membrane, and probed with an anti-GFP variant antibody. The positions of detected EYFP-HMW2, EYFP-P41, EYFP-P24, and ECFP-P65 are indicated by arrows. Molecular sizes are shown at left. (B) Western blot analysis of high-level expression transformants. Lysates of *M. pneumoniae* transformant cells (TK2100, TK2310T, TK2311T, and TK2310T) (5 μg of total protein) were analyzed under the same conditions in those used in panel A. The positions of detected fusion proteins are indicated by arrows.

were located at the proximal end of the organelle, suggesting that this site is the preferential localization site for both P41 and P24.

We also transformed *M. pneumoniae* M129 with the pMPN and pMPN-tuf plasmids, and the *eyfp-hmw2*, *eyfp-p41*, and *eyfp-p24* fusion genes were expressed (strains TK3310, TK3311, TK3312, TK3310T, TK3311T, and TK3312T). We confirmed that the localization patterns for EYFP-HMW2, EYFP-P41, and EYFP-P24 in the background of strain M129 were identical to those in the background of strain TK210 (Fig. 8A; only the images for TK3310T, TK3311T, and TK3312T are shown); these results indicate that the presence of ECFP-P65 does not affect the localization of these EYFP fusions.

DISCUSSION

Fluorescent-protein tagging is a widely used strategy for visualizing proteins in living cells. In this study, we have constructed vectors for fluorescent-protein tagging in *M. pneumoniae* and used them to visualize the protein components of cytoskeleton-like structures. The vectors constructed in this study are based on the Tn*4001*mod vector system (11, 22) and possess *M. pneumoniae p65* or *tuf* promoters for the expression of fluorescent target proteins. These two promoters allow for high and low levels of expression of target proteins and are helpful for enhancing the resolution of fluorescent images and assessing the patterns of localization of target proteins. We used EYFP and ECFP as fluorescent-protein tags and designed a coexpression procedure for these proteins. This procedure enabled dual labeling of two target proteins in living *M. pneumoniae* cells. Since *M. pneumoniae* cells are pleomorphic, it is sometimes difficult to judge the position of the attachment organelle in the cell. The dual-labeling method made it easier to ascertain the position of the organelle relative to the target protein. The first fluorescent protein can be used to label the organelle, while the second is used for the other target proteins.

Using our fluorescent-protein tagging method, we visualized the four proteins—P65, HMW2, P41, and P24—that are encoded in the *crl* operon (Fig. 1A). The P65 protein labeled with EYFP was localized at the attachment organelle (Fig. 2), confirming previous observations obtained by immunofluorescence microscopy (20, 48, 49). The localization of P65 at the organelle indicates that P65 is a component of the attachment organelle. However, neither the function of P65 nor its involvement in cytadherence is fully understood, mainly because of the lack of P65 mutant strains. It is known that P65 is present at reduced steady-state levels in mutant strains that lack any of the cytadherence accessory proteins—HMW1, HMW2, HMW3, and P30. In these mutant strains, the polar localization of P65 is partially disrupted, depending on the extent to which the P65 levels are reduced (2, 20, 52). The stability and polar localization of P65 are thought to be correlated. To stabilize P65, it may be necessary to incorporate it into the stable localization site at the organelle. This stable localization site may be provided by the other cytoskeletal proteins (25). Unincorporated P65 tends to be degraded by proteolysis. Consistent with this model, in strain TK162, expressing a high level of EYFP-P65, the level of native P65 was lower than the levels in the other strains (Fig. 3, lane 4). It is likely that the localization site for P65 at the organelle was occupied by an excess of EYFP-P65 in this strain and that unincorporated native P65 and EYFP-P65 were degraded. This sce-

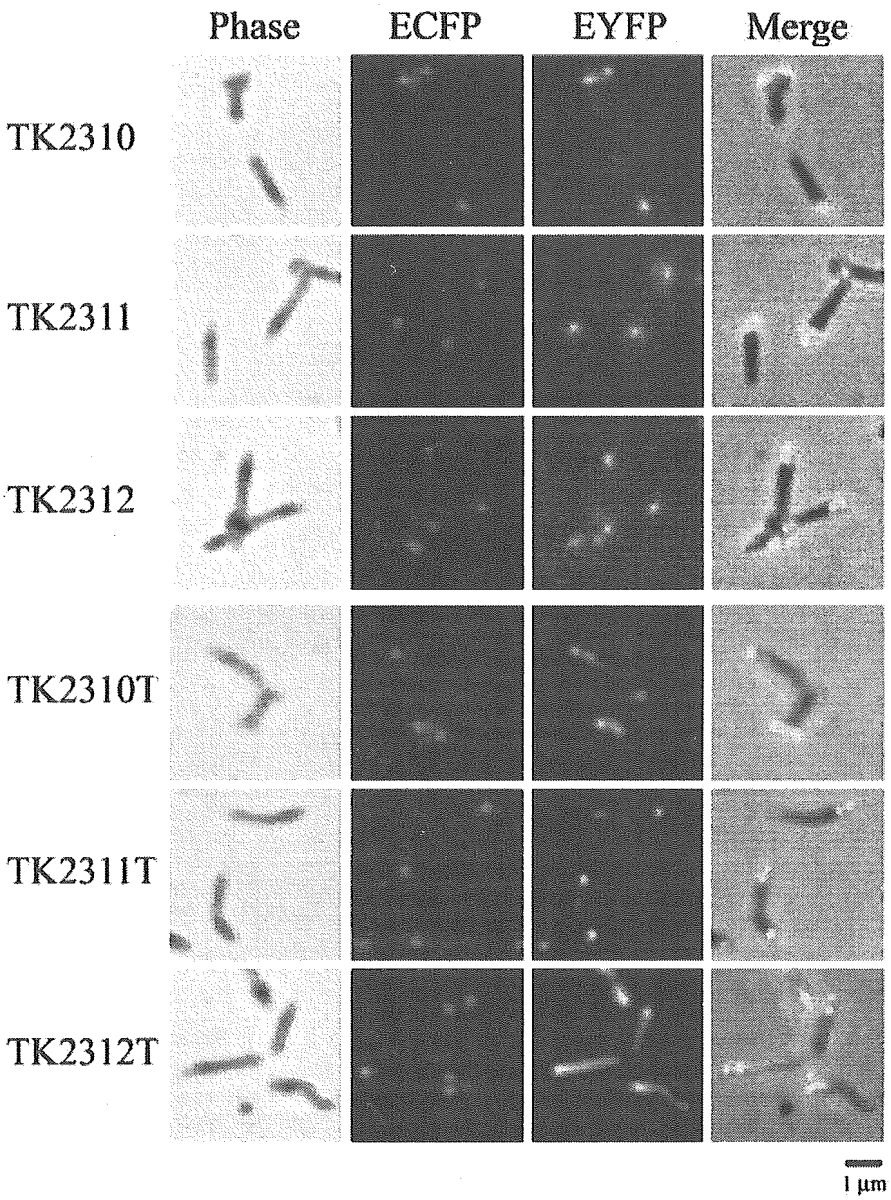

FIG. 7. Subcellular localization of EYFP-HMW2, EYFP-P41, and EYFP-P24 fusions in the *M. pneumoniae* TK210 cell background. Images of six *M. pneumoniae* transformants (names at left) are shown. The first panel in each row shows the phase-contrast image of the cells. The second and third panels in each row show ECFP and EYFP fluorescence images of the same cells, respectively. The fourth panel in each row shows the merged image of the phase-contrast and fluorescence images. Transformants TK2310, TK2311, and TK2312 show low levels of expression of EYFP-HMW2, EYFP-P41, and EYFP-P24, respectively; transformants TK2310T, TK2311T, and TK2312T show high levels of expression. Bar, 1 μm.

nario may also explain the clear focal fluorescence signals of EYFP-P65 at the attachment organelle and the lesser amounts of additional fluorescence in other parts of *M. pneumoniae* cells, even with high-level expression of EYFP-P65 (Fig. 2). Because EYFP-P65 gave clear focal fluorescence signals at the organelle, we also labeled P65 with ECFP and used ECFP-P65 as a positional marker of the organelle for examining the localizations of the other proteins (Fig. 5).

The HMW2 protein is a critical factor for cytadherence. It is thought to function in the early stage of assembly of the attachment organelle, together with the HMW1 protein (25). The loss of HMW2 affects the stability and polar localization of most of the other cytadherence accessory proteins, but HMW2 itself is also less stable in the absence of HMW1 (2). The EYFP-HMW2 fusion was localized at the attachment organelle when expressed at both high and low levels (Fig. 7), supporting the observations of Balish et al. (3). The localization sites for EYFP-HMW2 were almost identical to those for ECFP-P65 coexpressed in the same cells. However, in a considerable number of these cells, the fluorescence signals from EYFP-HMW2 extended slightly farther toward the proximal end than did the signals from ECFP-P65, which were relatively limited to the distal end of the organelle (data not shown). These observations agree with previous ones (49) and with the cur-

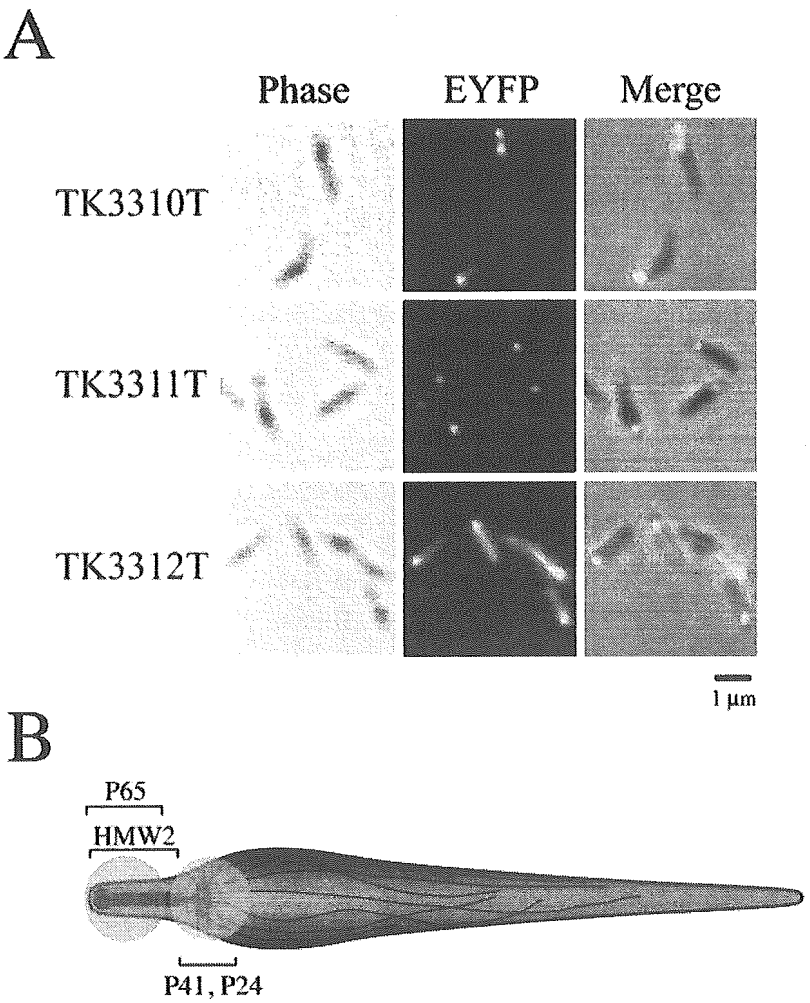

FIG. 8. (A) Subcellular localization of EYFP-HMW2, EYFP-P41, and EYFP-P24 fusions in the wild-type *M. pneumoniae* M129 cell background (without ECFP-P65). The left and middle panels in each row show images of the same cells observed by phase-contrast microscopy and fluorescence microscopy, respectively. The right panel in each row shows the merged image of the left and middle panels. The transformants are named at left. Bar, 1 μm. (B) Schematic illustration of an *M. pneumoniae* cell. Cytoskeleton-like structures within the *M. pneumoniae* cell (electron-dense core, wheel-like structure, and fibrous network) are illustrated (see the text). Approximate positions of the fluorescent signals observed by microscopy are shown with colors (blue, ECFP-P65; green, EYFP-P41 and EYFP-P24). Positions of sites of localization of P65, HMW2, P41, and P24 are indicated.

rent structural model of the organelle, which proposes that P65 is localized at the surface of the distal end of the attachment organelle and that HMW2 is the most probable component of the electron-dense core (25).

Little is known about the P41 and P24 proteins (25, 28). A homologous gene for P41 is present in the closely related species *Mycoplasma genitalium* (17), but no homologous gene has been found for P24. Although the functions of P41 and P24 are unknown, both attract considerable interest as cytoskeletal proteins, since they are encoded in the *crl* operon, together with P65 and HMW2, and are associated with the Triton shell (H. Ogaki et al., unpublished data). In addition, the P41 protein is predicted to contain a coiled-coil structure that has been observed in the other cytoskeletal proteins. Therefore, we analyzed the subcellular localization of these proteins by fluorescent-protein tagging and demonstrated that EYFP-P41 and EYFP-P24 were preferentially localized at the proximal end of the attachment organelle in *M. pneumoniae* cells, suggesting that they are cytoskeletal proteins that form unknown structures at this site. However, it should be noted that the high-level expression of both of these proteins exhibited additional fluorescent signals in the cells (Fig. 7). We thought that these additional localization patterns were caused by accumulations of excess proteins in the cells, but it remains possible that these localization patterns in cells with high-level expression reflect the native localization patterns for P41 and P24. This point must be assessed by using another method, such as immunofluorescence. If P41 and P24 really do localize to the proximal end of the attachment organelle, then what structures are present at this site? Recently, the presence of a wheel-like complex that might be part of a cytoskeleton-like structure was suggested at the proximal end of the electron-dense core by transmission electron microscopy of an ultrathin section of *M. pneumoniae* cells (16). This wheel-like complex is structurally

similar to the flagellar motor and might be connected to fibrous structures extending into the cytoplasm of *M. pneumoniae* cells. The detailed structure of this wheel-like complex has yet to be elucidated, but its position (at the proximal end of the electron-dense core) corresponds to the P41 and P24 localization site (Fig. 8B).

We also used the fluorescent-protein tagging technique to observe gliding *M. pneumoniae* cells (Fig. 4). The expression of EYFP-P65 in *M. pneumoniae* allowed real-time visualization of the attachment organelle of gliding cells by phase-contrast and fluorescence microscopy. The successful labeling of the attachment organelle of living *M. pneumoniae* cells indicated that this technique should be applicable to the direct observation of the cell division processes in *M. pneumoniae* (i.e., nascent organelle formation, the migration of one of the organelles to the opposite end, and cytokinesis) (34, 36, 48). However, an attempt at such an application was not successful in this study. The major reason for this result might have been the nutrient conditions of *M. pneumoniae* cells used for microscopy. We used saline containing 20% horse serum to suspend cells for fluorescence microscopy in order to reduce background fluorescence. Such low-nutrient conditions might not be sufficient to support cell division in *M. pneumoniae*. If cell division did somehow occur under these conditions, then a longer observation time might have been required, since the doubling time of *M. pneumoniae* M129 is estimated to be about 10 h, even under optimal conditions (31). In future studies, these situations could be improved by reducing the background fluorescence in the medium or by using fusion proteins with more intense signals.

ACKNOWLEDGMENTS

We are grateful to D. C. Krause of the University of Georgia for providing plasmid pKV104 and to C. Citti of the University of Veterinary Medicine, Vienna, Austria, for providing plasmid pISM2062.2. We thank Y. Arakawa of the National Institute of Infectious Diseases, Tokyo, Japan, for helpful input.

This work was supported in part by a Grant-in-Aid for JSPS Fellows from the Japan Society for the Promotion of Science (to S.S.) and by Grants-in-Aid for Young Scientists (to A.H.), for Scientific Research (to M.M.), and for Science Research on Priority Areas (motor proteins, genome science, and infection and host response) (to M.M.) from the Ministry of Education, Culture, Sports, Science, and Technology of Japan.

REFERENCES

1. **Aluotto, B. B., R. G. Wittler, C. O. Williams, and J. E. Faber.** 1970. Standardized bacteriologic techniques for the characterization of mycoplasma species. Int. J. Syst. Bacteriol. **20:**35–58.
2. **Balish, M. F., and D. C. Krause.** 2002. Cytadherence and cytoskeleton, p. 491–518. *In* S. Razin and R. Herrmann (ed.), Molecular biology and pathogenicity of mycoplasmas. Kluwer Academic/Plenum Publishers, New York, N.Y.
3. **Balish, M. F., R. T. Santurri, A. M. Ricci, K. K. Lee, and D. C. Krause.** 2003. Localization of *Mycoplasma pneumoniae* cytadherence-associated protein HMW2 by fusion with green fluorescent protein: implications for attachment organelle structure. Mol. Microbiol. **47:**49–60.
4. **Berg, H. C., and L. Turner.** 1993. Torque generated by the flagellar motor of *Escherichia coli*. Biophys. J. **65:**2201–2216.
5. **Biberfeld, G., and P. Biberfeld.** 1970. Ultrastructural features of *Mycoplasma pneumoniae*. J. Bacteriol. **102:**855–861.
6. **Bredt, W.** 1968. Motility and multiplication of *Mycoplasma pneumoniae*. A phase contrast study. Pathol. Microbiol. (Basel) **32:**321–326.
7. **Bredt, W.** 1973. Motility of mycoplasmas. Ann. N. Y. Acad. Sci. **225:**246–250.
8. **Dandekar, T., M. Huynen, J. T. Regula, B. Ueberle, C. U. Zimmermann, M. A. Andrade, T. Doerks, L. Sanchez-Pulido, B. Snel, M. Suyama, Y. P. Yuan, R. Herrmann, and P. Bork.** 2000. Re-annotating the *Mycoplasma pneumoniae* genome sequence: adding value, function and reading frames. Nucleic Acids Res. **28:**3278–3288.
9. **Feldner, J., U. Gobel, and W. Bredt.** 1982. *Mycoplasma pneumoniae* adhesin localized to tip structure by monoclonal antibody. Nature **298:**765–767.
10. **Green, G., S. R. Kain, and B. Angres.** 2000. Dual color detection of cyan and yellow derivatives of green fluorescent protein using conventional fluorescence microscopy and 35-mm photography. Methods Enzymol. **327:**89–94.
11. **Hahn, T. W., E. A. Mothershed, R. H. Waldo, and D. C. Krause.** 1999. Construction and analysis of a modified Tn*4001* conferring chloramphenicol resistance in *Mycoplasma pneumoniae*. Plasmid **41:**120–124.
12. **Hahn, T. W., M. J. Willby, and D. C. Krause.** 1998. HMW1 is required for cytadhesin P1 trafficking to the attachment organelle in *Mycoplasma pneumoniae*. J. Bacteriol. **180:**1270–1276.
13. **Hanahan, D.** 1983. Studies on transformation of *Escherichia coli* with plasmids. J. Mol. Biol. **166:**557–580.
14. **Hansen, E. J., R. M. Wilson, and J. B. Baseman.** 1979. Isolation of mutants of *Mycoplasma pneumoniae* defective in hemadsorption. Infect. Immun. **23:** 903–906.
15. **Hedreyda, C. T., K. K. Lee, and D. C. Krause.** 1993. Transformation of *Mycoplasma pneumoniae* with Tn*4001* by electroporation. Plasmid **30:**170–175.
16. **Hegermann, J., R. Herrmann, and F. Mayer.** 2002. Cytoskeletal elements in the bacterium *Mycoplasma pneumoniae*. Naturwissenschaften **89:**453–458.
17. **Himmelreich, R., H. Plagens, H. Hilbert, B. Reiner, and R. Herrmann.** 1997. Comparative analysis of the genomes of the bacteria *Mycoplasma pneumoniae* and *Mycoplasma genitalium*. Nucleic Acids Res. **25:**701–712.
18. **Hu, P. C., R. M. Cole, Y. S. Huang, J. A. Graham, D. E. Gardner, A. M. Collier, and W. A. Clyde, Jr.** 1982. *Mycoplasma pneumoniae* infection: role of a surface protein in the attachment organelle. Science **216:**313–315.
19. **Inamine, J. M., S. Loechel, and P. C. Hu.** 1988. Analysis of the nucleotide sequence of the P1 operon of *Mycoplasma pneumoniae*. Gene **73:**175–183.
20. **Jordan, J. L., K. M. Berry, M. F. Balish, and D. C. Krause.** 2001. Stability and subcellular localization of cytadherence-associated protein P65 in *Mycoplasma pneumoniae*. J. Bacteriol. **183:**7387–7391.
21. **Kirchhoff, H.** 1992. Motility, p. 473–489. *In* J. Maniloff, R. N. McElhaney, L. R. Finch, and J. B. Baseman (ed.), Mycoplasmas: molecular biology and pathogenesis. American Society for Microbiology, Washington, D.C.
22. **Knudtson, K. L., and F. C. Minion.** 1993. Construction of Tn*4001lac* derivatives to be used as promoter probe vectors in mycoplasmas. Gene **137:**217–222.
23. **Krause, D. C.** 1998. *Mycoplasma pneumoniae* cytadherence: organization and assembly of the attachment organelle. Trends Microbiol. **6:**15–18.
24. **Krause, D. C.** 1996. *Mycoplasma pneumoniae* cytadherence: unravelling the tie that binds. Mol. Microbiol. **20:**247–253.
25. **Krause, D. C., and M. F. Balish.** 2004. Cellular engineering in a minimal microbe: structure and assembly of the terminal organelle of *Mycoplasma pneumoniae*. Mol. Microbiol. **51:**917–924.
26. **Krause, D. C., and M. F. Balish.** 2001. Structure, function, and assembly of the terminal organelle of *Mycoplasma pneumoniae*. FEMS Microbiol. Lett. **198:**1–7.
27. **Krause, D. C., D. K. Leith, R. M. Wilson, and J. B. Baseman.** 1982. Identification of *Mycoplasma pneumoniae* proteins associated with hemadsorption and virulence. Infect. Immun. **35:**809–817.
28. **Krause, D. C., T. Proft, C. T. Hedreyda, H. Hilbert, H. Plagens, and R. Herrmann.** 1997. Transposon mutagenesis reinforces the correlation between *Mycoplasma pneumoniae* cytoskeletal protein HMW2 and cytadherence. J. Bacteriol. **179:**2668–2677.
29. **Layh-Schmitt, G., and R. Herrmann.** 1992. Localization and biochemical characterization of the ORF6 gene product of the *Mycoplasma pneumoniae* P1 operon. Infect. Immun. **60:**2906–2913.
30. **Layh-Schmitt, G., A. Podtelejnikov, and M. Mann.** 2000. Proteins complexed to the P1 adhesin of *Mycoplasma pneumoniae*. Microbiology **146:**741–747.
31. **Lipman, R. P., W. A. Clyde, Jr., and F. W. Denny.** 1969. Characteristics of virulent, attenuated, and avirulent *Mycoplasma pneumoniae* strains. J. Bacteriol. **100:**1037–1043.
32. **McBride, M. J.** 2001. Bacterial gliding motility: multiple mechanisms for cell movement over surfaces. Annu. Rev. Microbiol. **55:**49–75.
33. **Meng, K. E., and R. M. Pfister.** 1980. Intracellular structures of *Mycoplasma pneumoniae* revealed after membrane removal. J. Bacteriol. **144:**390–399.
34. **Miyata, M.** 2002. Cell division, p. 117–130. *In* S. Razin and R. Herrmann (ed.), Molecular biology and pathogenicity of mycoplasmas. Kluwer Academic/Plenum Publishers, New York, N.Y.
35. **Miyata, M., W. S. Ryu, and H. C. Berg.** 2002. Force and velocity of *Mycoplasma mobile* gliding. J. Bacteriol. **184:**1827–1831.
36. **Miyata, M., and S. Seto.** 1999. Cell reproduction cycle of mycoplasma. Biochimie **81:**873–878.
37. **Miyata, M., and A. Uenoyama.** 2002. Movement on the cell surface of the gliding bacterium, *Mycoplasma mobile*, is limited to its head-like structure. FEMS Microbiol. Lett. **215:**285–289.
38. **Miyata, M., H. Yamamoto, T. Shimizu, A. Uenoyama, C. Citti, and R. Rosengarten.** 2000. Gliding mutants of *Mycoplasma mobile*: relationships

between motility and cell morphology, cell adhesion and microcolony formation. Microbiology **146:**1311–1320.
39. **Phillips, G. J.** 2001. Green fluorescent protein—a bright idea for the study of bacterial protein localization. FEMS Microbiol. Lett. **204:**9–18.
40. **Proft, T., H. Hilbert, G. Layh-Schmitt, and R. Herrmann.** 1995. The proline-rich P65 protein of *Mycoplasma pneumoniae* is a component of the Triton X-100-insoluble fraction and exhibits size polymorphism in the strains M129 and FH. J. Bacteriol. **177:**3370–3378.
41. **Proft, T., H. Hilbert, H. Plagens, and R. Herrmann.** 1996. The P200 protein of *Mycoplasma pneumoniae* shows common features with the cytadherence-associated proteins HMW1 and HMW3. Gene **171:**79–82.
42. **Radestock, U., and W. Bredt.** 1977. Motility of *Mycoplasma pneumoniae*. J. Bacteriol. **129:**1495–1501.
43. **Razin, S., and E. Jacobs.** 1992. Mycoplasma adhesion. J. Gen. Microbiol. **138:**407–422.
44. **Razin, S., D. Yogev, and Y. Naot.** 1998. Molecular biology and pathogenicity of mycoplasmas. Microbiol. Mol. Biol. Rev. **62:**1094–1156.
45. **Regula, J. T., G. Boguth, A. Gorg, J. Hegermann, F. Mayer, R. Frank, and R. Herrmann.** 2001. Defining the mycoplasma 'cytoskeleton': the protein composition of the Triton X-100 insoluble fraction of the bacterium *Mycoplasma pneumoniae* determined by 2-D gel electrophoresis and mass spectrometry. Microbiology **147:**1045–1057.
46. **Romero-Arroyo, C. E., J. Jordan, S. J. Peacock, M. J. Willby, M. A. Farmer, and D. C. Krause.** 1999. *Mycoplasma pneumoniae* protein P30 is required for cytadherence and associated with proper cell development. J. Bacteriol. **181:**1079–1087.
47. **Sambrook, J., and D. W. Russell.** 2001. Molecular cloning: a laboratory manual, 3rd ed. Cold Spring Harbor Laboratory Press, Cold Spring Harbor, N.Y.
48. **Seto, S., G. Layh-Schmitt, T. Kenri, and M. Miyata.** 2001. Visualization of the attachment organelle and cytadherence proteins of *Mycoplasma pneumoniae* by immunofluorescence microscopy. J. Bacteriol. **183:**1621–1630.
49. **Seto, S., and M. Miyata.** 2003. Attachment organelle formation represented by localization of cytadherence proteins and formation of the electron-dense core in wild-type and mutant strains of *Mycoplasma pneumoniae*. J. Bacteriol. **185:**1082–1091.
50. **Southward, C. M., and M. G. Surette.** 2002. The dynamic microbe: green fluorescent protein brings bacteria to light. Mol. Microbiol. **45:**1191–1196.
51. **Stevens, M. K., and D. C. Krause.** 1991. Localization of the *Mycoplasma pneumoniae* cytadherence-accessory proteins HMW1 and HMW4 in the cytoskeletonlike Triton shell. J. Bacteriol. **173:**1041–1050.
52. **Willby, M. J., and D. C. Krause.** 2002. Characterization of a *Mycoplasma pneumoniae hmw3* mutant: implications for attachment organelle assembly. J. Bacteriol. **184:**3061–3068.
53. **Yanisch-Perron, C., J. Vieira, and J. Messing.** 1985. Improved M13 phage cloning vectors and host strains: nucleotide sequences of the M13mp18 and pUC19 vectors. Gene **33:**103–119.

第14改正 日本薬局方収載の【微生物関連】試験法設定と現場での適用

技術情報協会

1. 序文

「無菌試験」とは，規定された検体又は試料の量について，規定された培地を用い，規定された方法に従って試験したとき，検体又は試料に由来すると判断される微生物が検出されるかどうかを調べることである。現行の無菌試験培地には比較的広範囲にわたる各種の菌が発育するが，全ての菌が発育するわけではなく，ヒトに重篤な感染症を引き起こす可能性のある病原菌の中には無菌試験培地で発育しないものもある。また，無菌試験に供される検体や試料の量は限られており，汚染率が低く，汚染菌数が少ないときには，無菌試験で汚染菌を検出するのは不可能に近い。それ故，例え規定された無菌試験に合格しても，培地，検体量，試験方法を変えれば検出できるかも知れない微生物の存在までを否定するものではない。無菌試験とは，限られた範囲での無菌性を保証するための一手段にすぎず，無菌試験結果のみで製品の無菌性が保証されるものではない。GMP における無菌性保証の基本的考え方は，無菌性が十分にバリデートされている工程で製造され，かつ「無菌試験」にも適合することである。それ故，製品の無菌性は，一連の製造工程（滅菌工程，ろ過工程，充填工程，凍結乾燥工程，閉塞工程等）が完璧にバリデートされていることが不可欠であり，きわめて重要である。

1.1 無菌試験の感度

1970 年代には，「無菌とは単なる哲学的絶対概念に過ぎない。それは単に生きている微生物が全く存在しないことを想像しているだけである（Sterility is a simple philosophical absolute concept. It simply envisages the complete absence of viable microorganisms. Kelsey J.C. Lancet ii: 1301, 1972)」と言われたが，現在は「無菌とは生きている微生物が存在しない状態（State of being free from viable microorganisms)」と定義づけられている。無菌医薬品の製造方法は，最終容器に製品を充填，閉塞後，滅菌処理する最終滅菌法（Terminal sterilization）と，ろ過滅菌後又は原料調製段階から一連の無菌工程で製造する無菌操作法（Aseptic processing）に大別できる。前者の製法については，無菌性保証水準（SAL: sterility assurance level）が 10^{-6} 以下，後者については 10^{-3} 以下が求められている。例えば，汚染率 1％と 0.1％の母集団（ロット）から無作為に 20 個の検体を採取して無菌試験を実施したとする。容器の全量を培地に接種し，しかも 1 個の菌でも存在したら発育するものと仮定する。この場合，無菌試験によって汚染検体を検出できる確率は，式 1 から計算上，汚染率 1％では 18.2％，汚染率 0.1％では 1.98％である（表 1)。これは，汚染率 1％のロット製品でも 80％以上は汚染検体に遭遇できず合格扱いになることを示している。1％及び 0.1％の汚染母集団から 99％の確率で汚染菌を検出するとしたら，それぞれ実に 458 本及び 4,602 本を抜き取らなければならなくなる（表 2)。これは，培地

充填試験における充填容器数の考え方と同じである。すなわち，無菌試験における母集団の無菌性保証は，10～20%レベルであり，無菌性バリデーションが実施されている現状では，出荷時にセレモニー的に行っているに過ぎないとも言える。

$$P = 1 - (1 - x)^{n} \qquad (式1)$$

P：汚染検体検出確率，　X：汚染率，　n：抜き取り個数

表1　汚染検体検出率

汚染率（%）	汚染検体検出率（%）	
	10個	20個
10	65.13	87.84
1.0	9.56	18.20
0.1	0.99	1.98

汚染率の異なる母集団から無作為に10個または20個の検体を抜き取って無菌試験を行った場合の汚染検体検出率。

表2　汚染検体検出率と試験に必要な容器個数

汚染率（%）	検出率と抜き取り個数		
	99%	90%	80%
10	44個	22個	15個
1.0	458	229	160
0.1	4,602	2,301	1,608

1.2　国家検定「無菌試験」実績から推測する無菌性の推移

生物学的製剤（ワクチン，血液製剤等の総称）は，国民の健康に重要な位置を占めるため，薬事法第42条により，大臣が基準を制定し，品質についてはメーカーにおける自家試験の他に国が指定する機関（国立感染症研究所）で国家検定を実施している。国立感染症研究所の前身である国立予防衛生研究所が発足したのは，1947年で，翌年から国家検定が行われている。国立予防衛生研究所時代から現在に至るまでの国家検定無菌試験成績を図1に示す。図1より，国家検定制度が導入された頃は，約10%が無菌試験で不合格になっていた。10%の不合格というのは，現在の許容基準（SAL $< 10^{-3}$）から推測すると100%が汚染製剤であったと言える。当時の医薬品の無菌性は，無菌製造法によるものではなく，飽くまでも製剤に加えた防腐剤の効力に頼るものであった。しかし，1970年代になって急速に再試験率が減少している。これは，何と言ってもHEPAフィルターの導入により，無菌製造環境が著しく改善されたためである。

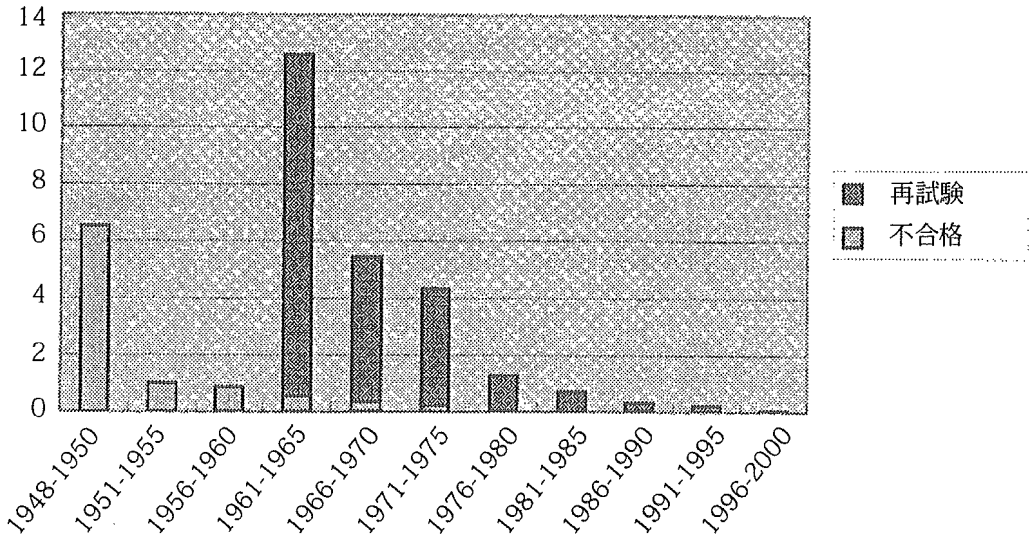

図1　国家検定無菌試験における不合格率及び再試験率（%）の推移

1.3　医薬品の細菌汚染と健康被害

医薬品の微生物汚染による健康被害を歴史的に振り返ると，圧倒的に多いのは血液製剤を介してのウイルス汚染である。細菌汚染による重篤な健康被害は，ロットを構成しない血液製剤（血漿，赤血球製剤，血小板製剤等）の使用によって起こることはあるが，一般医薬品の細菌汚染で重篤な健康被害を引き起こした事例を筆者は知らない。血液製剤の場合，細菌増殖を促す栄養素が豊富なため，細菌増殖には適していることと患者に大量に投与されることにある。細菌汚染成分血の輸血によって引き起こされる敗血症は，かなり高濃度に汚染した製剤を大量に輸血することにより，汚染菌や菌体成分で刺激を受けたマクロファージや血管内皮細胞が過剰に産生するTNFやIL-6，IL-8などの炎症性サイトカインが血流中に入り，敗血症カスケードを介して全身性の炎症反応を惹起することと解釈できる。図1から推測する限り，かなりの細菌汚染医薬品が市場に出てきたし，使われてもきた。しかし，医薬品の細菌汚染による健康被害報告が無かったのは，どうしてかという疑問に対しては，GMPが施行されていなかった時代でも感染を成立させるほどには，汚染の程度がひどくなかったためと考えられる。なお，無菌試験の感度は悪いとはいえ，汚染製剤の多かった時代には，無菌試験はそれなりに汚染レベルを低く抑える役割を果たしてきたことも事実である。

1.4　局方無菌試験法の歴史

無菌試験法は，1932年，英国薬局方（BP）に初めて導入され，USPには1936年，日局には1951年に導入されている。USP及び日局の無菌試験法の歴史を表3及び4に示す。日局「無菌試験法」は第12改正第二追補（1994）で大改正を行ったが，その後，国際調和の観点から見

直しが必要となり，第13改正第二追補（1999）で改正し，更に国際調和により，第14改正第二追補（2004）で改正がなされる。

表3　USPにおける無菌試験法の歴史

年	版	主な変更/改正点
1936	11	USPに初めて無菌試験法を導入（適用製剤は無菌液剤のみ）
1942	12	固形および液剤製品に対する好気性菌検出試験の導入，防腐剤の不活化について記載
1945	13	好気性菌および嫌気性菌の検出に液状チオグリコール酸培地の導入 カビおよび酵母の検出にハチミツ培地の導入 無菌試験実施環境および試験実施者のトレーニングについて記載
1950	14	液状チオグリコール酸培地の培養温度を37 Cから32-35 Cに変更 ハチミツ培地をサブロー培地に変更
1955	15	サブロー培地の組成を一部変更
1970	18	サブロー培地をソイビーン・カゼイン・ダイジェスト（SCD）培地に変更， メンブランフイルター（MF）法の導入， 無菌試験実施環境および試験実施者のトレーニングの項を充実
1975	19	MF法と直接法に分けて記載，大容量（>100 ml）液剤に対する試験方法も提示
1980	20	培地性能試験方法を導入，prefilled syringeに対する試験方法を導入，偽陽性と推定される試験結果に対しての再試験要件の記載，抗菌性物質に対する要件，医療用具に対する試験法および滅菌条件に対する項を導入
1985	21	再試験について要件を厳しくする，局方品目の無菌性保証に関するプロセスバリデーション概念の導入，無菌試験対象物に対する「ロット」概念を導入，無菌試験実施方法，観察方法，判定方法の項を充実
1990	22	MF法採用時における抗カビおよび抗菌活性の除去法を詳述，MF法全体の記述を充実
1995	23	22版の一部修正のみ
2000	24	全面改正：培地性能試験用菌株の入れ替え，試験のバリデーションの項を導入，抗菌活性物質の不活化，除去の限界について言及，供試検体数，接種量の見直し，試験実施施設にアイソレーターを追加，試験結果の解釈方法について見直し

表4　日局における無菌試験法の歴史

年	版	主な変更/改正点
1951	6	日局に初めて無菌試験法を導入（適用製品は注射用蒸留水および滅菌蒸留水）．全体的に培地に関する記述が多く，解説書的内容．
1961	7	解説書的内容を一新し，試験法の体裁を整えた．細菌試験と真菌（カビおよび酵母）試験に分けて記載．細菌試験には液状チオグリコール酸培地，真菌試験にはブドウ糖・ペプトン培地を使用．接種量および培地量も記載．液状チオグリコール酸培地の培地性能試験菌株として*Clostridium tetani*（破傷風菌）および*Streptococcus haemolyticus*（溶血性連鎖球菌）を指定．
1971	8	無菌試験実施環境として，無菌箱または無菌室内を提示．「試料の取り方」の項を削除
1976	9	液状チオグリコール酸培地IIを導入．無菌試験実施環境として無菌箱または無菌設備内を提示．*Clostridium tetani*および*Streptococcus haemolyticus*を培地性能試験菌株の指定から外す
1981	10	MF法を導入（試験は別に規定するもののほか，直接法により行う，MF法は表示量または調製量100 ml以上のものに適用）．細菌試験と真菌試験をまとめて記載．試験実施者の要件を提示．
1986	11	変更，追加等なし
1994	12	全面改正．グルコース・ペプトン培地をSCD培地に変更，培養期間をMF法直説法ともに14日間以上に変更，培地性能試験菌株を指定，微生物発育阻止物質の試験および除去方法を導入，判定方法を明記

2. 無菌試験法の国際調和

1990年代は，日米欧3極で医薬品規制に関する種々のガイドライン作成，薬局方試験法並びに医薬品各条の調和作業が大いに進展した時代でもある。1991年に設立された医薬品承認審査ハーモナイゼーション国際会議（ICH：International Conference on Harmonization of Technical Requirements for Registration of Pharmaceuticals for Human Use）は，日米欧の行政機関（EU, FDA, 厚労省）と製薬業界代表（EFPIA, PhRMA, JPMA）からなり，医薬品の承認審査時における安全性，品質，効力評価に必要な試験手法について3極（日米欧）で議論することを目的に発足した。以来，ICHは積極的な活動を続け，多くのガイドラインを出してきた。それらの原文及び翻訳版は，国立医薬品食品衛生研究所のウエーブサイト（http://www.nihs.go.jp/index-j.html）から入手可能である。日米欧薬局方の試験法及び医薬品各条（主に添加剤）の調和作業は，1990年に設立された薬局方検討会議（PDG：Pharmacopoeial Discussion Group）で行われている。薬局方試験法の調和（harmonization）とは，「A pharmacopoeial general chapter or other pharmacopoeial document is harmonized when a pharmaceutical substance or product tested by the procedure yields the same results, and the same accept/reject decision is reached：薬局方に収載されている物質又は製品について，当該手法によって試験したとき，同じ結果，同じ合否判定に達する場合，一般試験法又は局方各条は調和されている」と定義づけられている。無菌試験法の国際調和作業は，EPが事務局を担当し，1995年から作業を開始し，調和署名がなされたのは，7年後の2002年であった。国際調和がなされたとは言え，多くの点で3薬局方の考え方に違いが生じた。これらの違いを含め，国際調和無菌試験法を反映して作成された日局無菌試験法（3）（第十四改正日本薬局方第二追補：2004年12月）を中心に以下，解説する。

2.1 無菌試験実施環境

試験環境は，無菌試験の実施に適していなければならない。

通常，無菌試験はグレードB環境に設置したクリーンベンチ，グレードC/D環境に設置されたアイソレータ又は閉鎖系ロボットシステム，またはグレードA環境のクリーンルームで行われる。クリーンベンチ又はセーフティキャビネットのいずれも無菌試験に適用できるが，セーフティキャビネットよりはクリーンベンチの方が使い勝手はよい。セーフティキャビネットはその使用目的（バイオハザード対策）上，前扉を大きく開けることができないため作業は必ずしも容易ではない。いずれも作業面は容易に消毒できるタイプのものが望ましく，滴下した試料，培地などの除去，洗浄の困難なものは避けた方がよい。空気清浄度の表し方も種々あり，関係者間でも混乱をきたしている。最終的には国際規格（ISO 14644-1）に準拠したものに整理されていく

ものと思われるが，清浄度クラスの呼称，各クラスにおける許容微粒子数，許容浮遊微生物数について表５～７に示す。

表５　空気清浄度に関する各種基準の比較

ISO クラス*	下記に示すサイズ以上の微粒子が１m³中に存在する最大濃度						各種相当基準			
							米国連邦規格		英国規格	EU GMP
	0.1 μ m	0.2 μ m	0.3 μ m	0.5 μ m	1 μ m	5 μ m	209E	209D	5295	
ISO Class 1	10	2								
ISO Class 2	100	24	10	4						
							M1			
ISO Class 3	1000	237	102	35	8		M1.5	1	(C)	
							M2			
ISO Class 4	10 000	2 370	1 020	352	83		M2.5	10	(D)	
							M3			
ISO Class 5(L)	100 000	23 700	10 200	3520	832	29	M3.5	100 (L)	E	A
ISO Class 5(T)	100 000	23 700	10 200	3520	832	29	M3.5	100 (T)	F	B
							M4			
ISO Class 6	1 000 000	237 000	102 000	35 200	8 320	293	M4.5	1 000	G or H	
							M5			
ISO Class 7				352 000	83 200	2 930	M5.5	10 000	J	C
							M6			
ISO Class 8				3 520 000	832 000	29 300	M6.5	100 000	K	D
							M7			
ISO Class 9				35 200 000	8 320 000	293 000			L	

＊：ISO 14644-1 規格，L：層流又は一方向流，T：乱流又は非一方向流

表６　無菌医薬品製造環境の空気清浄度

ISO クラス	非作業時		作業時	
	空気１㎥中当たりの最大許容微粒子数			
	0.5 μ m	5 μ m	0.5 μ m	5 μ m
Class 5 (L)	3 500	30	3 500	30
Class 5 (T)	3 500	30	35 000	300
Class 6	35 000	300	350 000	3 000
Class 7	350 000	3 000	3 500 000	30 000
Class 8	3 500 000	30 000	35 000 000	300 000
Class 9	35 000 000	300 000	規定なし	規定なし

表 7　空気清浄度と環境微生物の評価基準

ISO クラス	微生物汚染に対する推奨許容基準			
	Air sample cfu/m^3	Settle plates (ϕ 90mm) cfu/4hours	Contact plates (ϕ 55mm) cfu/plate	Glove print 5 fingers cfu/glove
Class 5 (L)	＜1	＜1	＜1	＜1
Class 5 (T)	10	5	5	5
Class 6	50	25	10	—
Class 7	100	50	25	—
Class 8	200	100	50	—
Class 9	規定なし	規定なし	規定なし	規定なし

2.2　培地及び洗浄液の調製法

培地は別に規定する場合を除き，通例，液状チオグリコール酸培地及びソイビーン・カゼイン・ダイジェスト培地を用いる。試料の混濁又は粘性のために，液状チオグリコール酸培地が使用しにくいときは，変法チオグリコール酸培地を用いてもよい。ただし，変法チオグリコール酸培地を用いるときは，使用直前に水浴上で加熱し，嫌気条件下で培養する。また，これらの成分を有する適当な品質の製品を用いてもよい。変法チオグリコール酸培地は，日本では全血の無菌試験に，USP ではチューブ（医療用具）内の無菌性を調べるために用いられている。現行の無菌試験培地には比較的広範囲にわたる各種の菌が発育するが，全ての菌が発育するわけではなく，発育しない菌も多い。例えば，筆者が経験した一例として，国家検定に供された生ワクチン製剤について無菌試験を行ったところメーカーの自家試験では適合であったのに対して，国家検定では試験した検体の全数で汚染を確認したことがある。汚染菌は，*Bradyrhizobium japonicum* という好気性の根瘤細菌であった。好気性菌なら SCD 培地で増殖しても良いのではと思われるかもしれないが，本菌は栄養学的に SCD 培地中では発育できない菌であった。本菌は滅菌後，数日おいた液状チオグリコール酸培地では増殖可能であった。メーカーでは，培地滅菌後直ちに無菌試験を行っていたのに対し，国家検定では 5 日間おいてから無菌試験を行っていた。この違いが汚染菌を検出できたかどうかの違いであった。その後，本汚染菌はブドウ糖ペプトン培地中では良く増殖することが分かったので，汚染原因の究明にはブドウ糖ペプトン培地を用いた。このように，現行無菌試験用培地は混入の可能性のある全ての汚染菌を検出するには十分なものではないが，一定レベルの汚染菌を検出するという目的にはかなった培地である。

液状チオグリコール酸培地の歴史

1940 年に Brewer（1）が，以下の組成からなるチオグリコレート培地を開発した。

Pork infusion solid　　1%

Peptone (thio)　　1%

Sodium chloride	0.5%
Sodium thioglycollate	0.1%
Agar	0.05%

本培地は好気条件下で嫌気性菌の増殖を可能にし，さらに生物製剤に防腐剤として添加されていたチメロサールを中和する能力があることが実証され，以後，無菌試験用培地として使用されるようになった。その後，TG 培地の成分を種々検討し，現在の組成を提案したのは米国 NIH の Pittman 女史(2)であった。Pittman 女史の提唱した TG 培地は，1947 年に USP VIII に採用され，以後，無菌試験培地として世界中の基準に採用されるようになった。1955 年に L-cystine 含量を 0.75g から 0.5g に減少した以外は，現行培地組成と全く同じである。

2.3 培地の適合性

無菌試験に供する培地についても 3 薬局方で意見が分かれた。EP は規定された培地性能試験に適合する培地なら何を用いてもよい表現をとった。一方，日局と USP は液状チオグリコール酸培地と SCD 培地にした。日局は無菌試験法を薬事法に基づいた出荷判定試験として捉えているので，培地の選択性を日局ユーザーの自由に託すわけにはいかない。勿論，全血などの無菌性を評価する培地は別の培地の方が良いことは知ってはいるが，日局対象医薬品をベースに考えると液状チオグリコール酸培地と SCD 培地の使用は必須である。ただし，医薬品の許可申請時等において，「規格及び試験法」に日局指定培地より他の培地の使用が科学的に妥当であることを示すことができるならば，日局指定以外の培地使用も不可能ではない。培地の適合性は，1）培地の無菌性と 2）培地の性能試験から成り立っている。

2.4 培地の有効期間

> 密封容器に入っている培地は，使用前 3 箇月以内に培地の性能試験を行い，基準を満たしているならば，調製後 1 年間使用できる。非密封容器に入っている培地は，使用前 2 週間以内に培地の性能試験を行い，基準を満たしているならば，調製後 1 箇月間使用できる。

培地性能試験は，被検体の無菌試験と同時に行うことができる。ただし，培地性能試験結果が不適合になった場合には，当該検体に対する無菌試験も無効になる。このことを念頭に入れて解釈していただければよい。密封容器に入った培地の場合は，文字通りの解釈で良いが，非密封容器に入った培地の性能試験が理解しがたいかも知れない。要は，無菌試験の培養期間 2 週間を考慮し，無菌試験は遅くとも培地調製後，2 週間目には行わなければならない。培地性能試験と